bradscholars

Biodegradable Polymer Composites of Metal Organic Framework-5 (MOF-5) for the Efficient and Sustained Delivery of Cephalexin and Metronidazole

Item Type	Article
Authors	Anim, Anoff;Mahmoud, L.A.M.;Kelly, Adrian L.;Katsikogianni, Maria;Nayak, Sanjit
Citation	Anim A, Mahmoud LAM, Kelly AL, et al (2023) Biodegradable Polymer Composites of Metal Organic Framework-5 (MOF-5) for the Efficient and Sustained Delivery of Cephalexin and Metronidazole. Applied Sciences. 13(19): 10611
DOI	https://doi.org/10.3390/app131910611
Rights	© 2023 The authors. Licensee MDPI, Basel, Switzerland. This article is an open access article distributed under the terms and conditions of the Creative Commons Attribution (CC BY) license (https://creativecommons.org/licenses/by/4.0/)
Download date	2026-02-18 18:28:47
Link to Item	http://hdl.handle.net/10454/20158

applied sciences

MDPI

Article

Biodegradable Polymer Composites of Metal Organic Framework-5 (MOF-5) for the Efficient and Sustained Delivery of Cephalexin and Metronidazole

Anoff Anim [1], Lila A. M. Mahmoud [1,2], Adrian L. Kelly [3], Maria G. Katsikogianni [1] and Sanjit Nayak [1,*]

[1] School of Chemistry and Biosciences, University of Bradford, Bradford BD7 1DP, UK; a.anim@bradford.ac.uk (A.A.); l.mahmoud@bradford.ac.uk (L.A.M.M.); m.katsikogianni@bradford.ac.uk (M.G.K.)
[2] School of Pharmacy, Al-Zaytoonah University of Jordan, Amman 11733, Jordan
[3] Polymer IRC, Faculty of Engineering and Informatics, University of Bradford, Bradford BD7 1DP, UK; a.l.kelly@bradford.ac.uk
* Correspondence: s.nayak@bradford.ac.uk

Abstract: The sustained and controlled delivery of antimicrobial drugs has been largely studied using nanomaterials, like metal organic frameworks (MOFs), and various polymers. However, not much attention has been given to combining MOFs and biodegradable polymers towards the potentially more sustained release of active pharmaceutical ingredients. Herein, we report a comparative study of two widely used antimicrobial drugs, cephalexin and metronidazole, from zinc-based MOF-5 incorporated into biodegradable polycaprolactone (PCL) and poly-lactic glycolic acid (PLGA) composites. Cephalexin and metronidazole were separately loaded into MOF-5 post-synthetically, followed by their integration into biodegradable PLGA and PCL composites. The pristine MOF-5 and the loaded MOFs were thoroughly characterised using Fourier-transformed infrared (FT-IR) spectroscopy, scanning electron microscopy (SEM), thermogravimetric analysis (TGA) and powder X-ray diffraction (PXRD). Ultraviolet-visible (UV-Vis) spectroscopy studies were carried out to assess the release of the drugs in PBS for up to 72 h, showing a cumulative release of 24.95 wt% and 27.84 wt% for cephalexin and metronidazole, respectively. The antibacterial properties of the pristine MOF, pure drugs, drug-loaded MOFs and the loaded composites were assessed against Gram-positive and Gram-negative bacterial strains, *Staphylococcus aureus* or *Staphylococcus epidermidis* and *Escherichia coli* or *Acinetobacter baumanii*, respectively. A cephalexin-loaded MOF-5 composite of PCL (PCL-ceph@MOF-5) showed the best efficiency for the controlled release of drugs to inhibit the growth of the bacteria compared to the other composites. This study demonstrates that the combination of MOFs with biodegradable polymers can provide an efficient platform for the sustained release of antimicrobial drugs and can be a promising tool to manage antimicrobial resistance (AMR).

Keywords: metal organic frameworks; biodegradable composites; antibacterial; antimicrobial resistance; cephalexin; metronidazole; MOF-5; PCL; PLGA

check for updates

Citation: Anim, A.; Mahmoud, L.A.M.; Kelly, A.L.; Katsikogianni, M.G.; Nayak, S. Biodegradable Polymer Composites of Metal Organic Framework-5 (MOF-5) for the Efficient and Sustained Delivery of Cephalexin and Metronidazole. *Appl. Sci.* **2023**, *13*, 10611. https://doi.org/10.3390/app131910611

Academic Editors: Mohamed Abdelaty Habila and Zeid Abdullah ALOthman

Received: 5 August 2023
Revised: 18 September 2023
Accepted: 20 September 2023
Published: 23 September 2023

Copyright: © 2023 by the authors. Licensee MDPI, Basel, Switzerland. This article is an open access article distributed under the terms and conditions of the Creative Commons Attribution (CC BY) license (https://creativecommons.org/licenses/by/4.0/).

1. Introduction

Antimicrobial resistance (AMR) is a major threat that compromises the efficacy of antimicrobial drugs and thereby increases the prevalence of diseases in both developed and developing countries [1]. In recent studies, it has been estimated that AMR will be the leading cause of deaths for about 10 million people worldwide, annually, by 2050 [2]. Increasing AMR can be partly attributed to the unnecessary oral administration of drugs, especially in cases of prolonged therapy, which often continues for a long period of time. To address the AMR crisis, various strategies, including reduction of the excess use of antimicrobial drugs and optimisation of dosages and the duration of therapies are being studied [3]. Although these strategies are applicable, they are rather long-term approaches,

and it will take time before a significant impact is seen against the rising cases of AMR. However, using a controlled and sustained drug delivery system of antimicrobials has been proposed as a promising strategy for the reduction of AMR [4,5]. This approach is about releasing the incorporated drugs in optimised concentrations at the targeted sites, minimising the need for frequent oral administration, which is one of the major contributors to AMR. In previous studies, various materials have been studied for the controlled release of drugs, and these include microcapsules, dendrimers, mesoporous silica, liposomes, organic micelles, quantum dots and biodegradable polymers [6–8]. However, these materials have various limitations, including uncontrolled degradation, low loading capacities and instability [9,10]. Recently, the use of metal organic frameworks (MOFs) as an alternative platform for the controlled release of drugs has proven to be promising [11,12]. MOFs are a class of hybrid crystalline materials formed from coordination bonds between metal ions crosslinked with organic linkers to form a two- or three- dimensional lattice with potential voids [13]. MOFs may contain micropores, which can be adjusted to various sizes with desired functional groups [14–16]. MOFs have therefore gained much attention due to their ultrahigh porosity, large surface area, thermal stability and high chemical selectivity, which makes them ideal for many applications, including chemical sensing, catalysis, supercapacitors and so on [17–22].

Recently, MOFs have caught much attention as a vehicle for antimicrobial drug delivery mainly because of their ability to provide the controlled release of different antimicrobial drugs, which is sometimes coupled with the release of metal ions, such as Ag^{+}, Co^{2+}, Zn^{2+} and organic linkers, to further enhance the antimicrobial effects of those systems [4,23–25]. The ions and linkers released can act through various mechanisms. For example, some of these antimicrobial agents perforate the bacterial cell wall and interfere with the synthesis of the nucleic acids of the bacterial cell, thereby destroying the bacteria [26,27]. However, some metal ions, like Ag^{+} and Co^{2+}, can be toxic to human cells, hence limiting their applications in drug delivery [4,28]. After considering this, a more biocompatible zinc-based MOF-5 has been chosen for drug delivery applications in this study, to avoid metal ion-based toxicity [5]. The chemical bonds between MOFs and the drugs include coordination bonds, hydrogen bonds and Van der Waals interactions [29,30].

Additionally, the powder form of MOFs is a major limitation, especially in drug delivery applications, and hence, incorporating them into biodegradable polymers makes them easily applicable [31]. The instability of MOFs is another limitation, which can be attributed to the reversibility of the coordination bonds [32]. Biodegradable polymers, including poly lactic-co-glycolic acid (PLGA) and polycaprolactone (PCL), have demonstrated the sufficient controlled release of drugs in previous studies [33–35]. These two polymers have varying degradability rates. Due to the semi-crystalline structure of PCL, it shows slower degradation compared to PLGA, which is amorphous [36]. This allows for the exploration of different types of biomedical applications for these two polymers based on their release behaviour facilitated by degradation [37]. Both MOFs and biodegradable polymers have significantly demonstrated the relevant controlled release of drugs in previous studies [31,35,38]. However, not much attention has been given to the combination of these two systems, biodegradable polymers and MOFs, for drug delivery applications. In this study, we took advantage of the combination of the two. Given their varying degradability rates, combining both, by encapsulating the MOFs into the polymers, gives an extended, slower release of the loaded drug in gradual, sustained and significant concentrations.

This study demonstrates a combined loaded MOF-polymer approach, firstly by loading zinc-based MOF-5 with a first-class antimicrobial, metronidazole (Met), to form met@MOF-5 and a cephalosporin beta-lactam antibiotic drug, cephalexin (Ceph), to make ceph@MOF-5. These loaded MOFs were then incorporated into biodegradable PLGA and PCL polymers to form PLGA-met@MOF-5, PLGA-ceph@MOF-5, PCL-met@MOF-5 and PCL-ceph@MOF-5 composite materials. After synthesis and formulation, the composite materials were characterised using thermogravimetric analysis (TGA), powder X-ray diffraction (PXRD), Fourier-transformed infrared (FTIR) and scanning electron

microscopy (SEM). To confirm the retention of the antibacterial properties of the combined nanocomposites, their activity was tested against both Gram-negative and Gram-positive bacteria, *Escherichia coli* or *Acinetobacter baumamiii* and *Staphylococcus aureus* or *Staphylococcus epidermidis*, respectively [39].

The varying degradability rates of PLGA and PCL account for different drug-release profiles, while Met and Ceph present different effectiveness against the selected bacterial strains of this study.

As such, we herein report a comparative study involving the loading and release of the Met and Ceph drug molecules using zinc-based MOF-5 and biodegradable PLGA and PCL polymers (Scheme 1), as an efficient combination to provide more sustained, controlled drug release relative to using MOFs or polymers independently for drug delivery purposes.

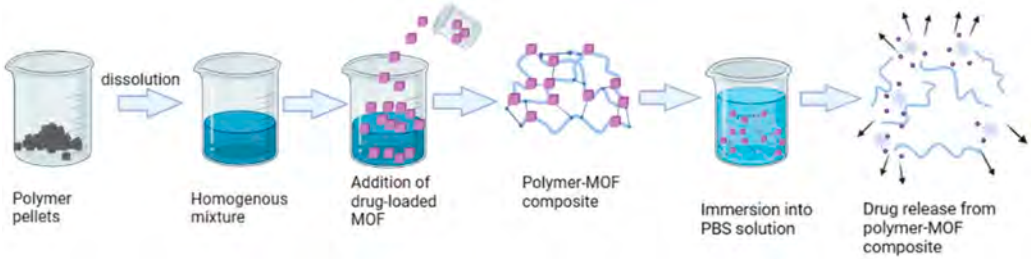

Scheme 1. Schematic illustration of the synthesis of polymer–MOF composites and drug release.

2. Experimental Section

2.1. Materials Used

All chemicals and reagents were purchased from Sigma-Aldrich, and the solvents were from Fisher Scientific. All chemicals were used in the state purchased without any further purification.

2.2. Synthesis

2.2.1. Synthesis of Pristine MOF-5

Previous works, as reported in the literature, were followed for the synthesis of MOF-5 with few modifications [30]; 0.166 g (1 mmol) of terephthalic acid (H_2BDC) and 0.297 g of $Zn(NO_3)_2{\cdot}6H_2O$ were dissolved in 5 mL of dimethylformamide (DMF). Two drops of triethylamine (TEA) were added to the resulting mixture using a syringe. The mixture was then sonicated and placed in a programmable oven at 120 °C for 24 h, with a heating rate of 5 °C min^{-1}, and cooling to 25 °C, at a cooling rate of 2 °C min^{-1}. The resultant white precipitate was filtered using vacuum filtration via a Büchner funnel. The precipitate was then washed multiple times with DMF and then placed in an oven at 80 °C to dry for 2 h.

2.2.2. Activation of MOFs

Solvent exchange was first performed by immersing MOFs in methanol for 30 min, and they were then filtered and dried in an oven. The dried MOFs were then activated in a vacuum oven at 115 °C for 24 h.

2.2.3. Post-Synthetic Loading of MOFs (Ceph@MOF-5 and Met@MOF-5)

Stock solutions of metronidazole (Met) and cephalexin (Ceph) were prepared separately by dissolving 1.2 g of each drug in 100 mL of DMF. Subsequently, in two other separate vials, 0.05 g of pristine and activated MOF-5 crystals were dissolved in 10 mL of each of the drug stock solutions and stirred at 800 rpm for 24 h. Cloudy suspensions were formed and centrifuged at 4350 rpm for 10 min. Then, 10 mL of DMF was used to wash the precipitates three times and placed in an oven at 80 °C to dry for 4 h. A Met stock solution was used to synthesise met@MOF-5, while a Ceph stock solution was used to synthesise ceph@MOF-5.

2.3. Formulation of Polymer Composites (PLGA-Ceph@MOF-5, PLGA-Met@MOF-5, PCL-Met@MOF-5 and PCL-Ceph@MOF-5)

A clean beaker containing 15 mL of chloroform was used to dissolve 0.2 g of PLGA and PCL pellets separately, via continuous stirring using a magnetic stirrer for 30 min. Then, 0.005 g of MOFs was ground using a mortar and pestle, and the grounded powder was added to each of the chloroform–polymer solutions. These mixtures were stirred continuously for about 20–25 min, until they formed homogeneous solutions. The solutions were then poured into silicone moulds and left to dry for 12 h at room temperature. The dried films were then peeled off and kept in a vial.

2.4. Material Characterisation

The Fourier-transformed infrared (FTIR) spectra of the pristine samples and the loaded samples were recorded over a range of 600 cm^{-1} to 4000 cm^{-1} with the use of a PerkinElmer spectrum 100 FTIR spectrometer, which is also fitted in a PerkinElmer universal ATR sampling device. The Q Series-[Q5000-0140] TGA instrument was used for the thermogravimetric analysis (TGA) of the samples. The crystals were heated using platinum pans from 30 °C up to 600 °C at a 5 °C min^{-1} heating rate with a continuous flow of nitrogen at a flow rate of 25 mL min^{-1}. The analysis of the data was performed using the TA Instrument's universal analysis 2000 Software. Powder X-ray diffraction (PXRD) data were recorded using a D8 Discover Bruker diffractometer with Cu Kα1,2-radiation (λ = 0.154018 nm, 1600 W) at an ambient temperature, and Origin was used for the analysis of diffraction patterns.

Images of scanning electron microscopy (SEM) and energy dispersive X-ray (EDX) data were collated using an FEI Quanta 400E-SEM with an Oxford Xplore 30 EDS system. Drug release studies were performed using a Jena UV-Vis spectrometer, to measure and record all the electronic absorbance spectra of the drug release study solutions.

2.5. Drug Release Studies

Release studies were performed in sink conditions using PBS as a medium. These were carried out by placing 5 mg of the loaded MOF into a 30 mL beaker and 20 mg of the loaded polymer–MOF composites into another beaker. Then, 20 mL of PBS solution was kept in a 37 °C water bath to be equilibrated, and this was later added to the samples in the respective beakers and left for 6 days. Samples of 2 mL aliquots were drawn from the supernatant after each day for 6 days. The aliquots drawn each day were replaced with 2 mL of fresh PBS, while the absorbance of the drawn aliquots was measured using the UV-vis spectrophotometer.

A calibration curve (Figures S1 and S2 in Supplementary Materials) was then prepared from control samples of Met and Ceph drugs with known concentrations within the concentration range of 0.0005 mg/mL to 0.3 mg/mL in PBS. The drug solutions were well stirred and sonicated to ensure the complete dissolution of Met and Ceph.

2.6. Antibacterial Studies

The antibacterial properties of the loaded MOFs and composites were assessed by testing them against 4 bacterial strains: Staphylococcus aureus (NCTC 6571), *Staphylococcus epidermidis*-(NCIZMBC 8853) *Escherichia coli* (NCTC 12923) and *Acinetobacter baumannii*-(ATCC 19606). The bacterial cultures were prepared overnight on Tryptic Soy Agar (TSA). Two to three colonies were then diluted in distilled and sterile water, and the turbidity was adjusted to 5×10^8 colony forming units (CFUs) mL^{-1} according to the McFarland standard [40]. The diluted bacterial suspensions were then spread onto the Mueller Hinton (MH) agar plates. Subsequently, the weighed (1 mg) samples of MOFs and their composites were carefully placed on the plate. The plates were then incubated for 24 h at 37 °C, before being imaged [41].

The zones of bacterial growth inhibition, in the individual Petri dishes, for the various bacterial strains were measured and recorded. The testing was repeated three times to

confirm its repeatability, and the average zones of inhibition, along with their standard deviation, were evaluated.

3. Results and Discussion

3.1. PXRD

PXRD data were collected and compared with the calculated pattern for MOF-5 to investigate the crystallinity and phase purity of pristine MOF-5, met@MOF-5 and ceph@MOF-5, as shown in Figure 1. The PXRD patterns of the pristine MOF-5 were found to be consistent with those reported in literature, confirming the phase purity [41].

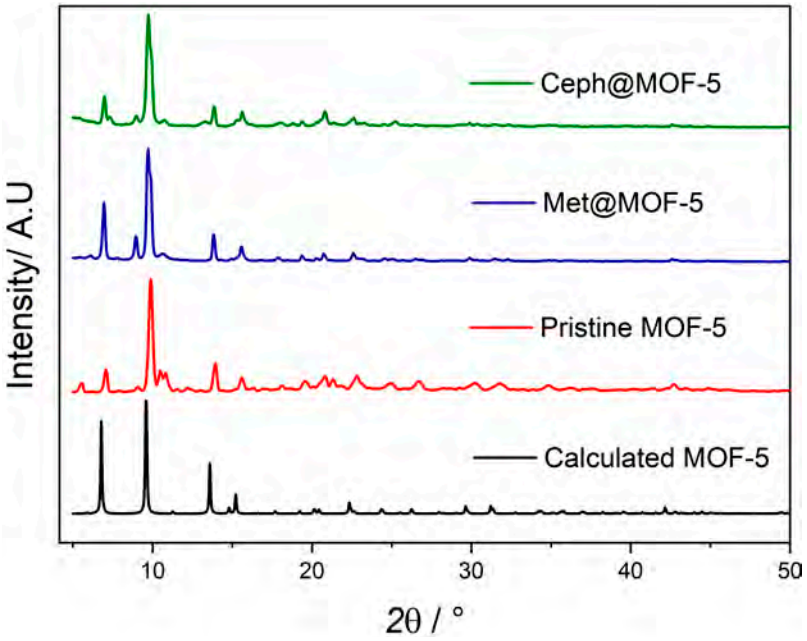

Figure 1. PXRD patterns of pristine MOF-5 (red) compared with the calculated patterns (black), met@MOF-5 (blue) and ceph@MOF-5 (green).

The PXRD patterns of met@MOF-5 appeared similar to the pristine MOF and showed all characteristic peaks of the pristine MOF-5, indicating that the crystal structure of the MOF after drug loading remained largely unaffected and the presence of the drug molecules did not alter the lattice parameters of the MOF [42,43].

The XRD patterns of ceph@MOF-5 also demonstrated very similar diffraction patterns, as compared to the patterns of the pristine MOF-5 and met@MOF-5. This indicates that the crystallinity of the MOF-5 was unaffected by the presence of the Ceph drug molecules [44]. This showed all the major and minor peaks of the pristine MOF-5 as shown in Figure 1. However, the absence or broadening of PXRD peaks for MOF-5 were noted after exposures of the drug-loaded MOF composites in PBS for 24 h (Figure S6 in Supplementary Materials).

3.2. SEM

The particle morphologies of the samples, as assessed by a comparison of SEM images of MOF-5, met@MOF-5 and ceph@MOF-5, are displayed in Figure 2. The pristine MOF-5 showed a regular rectangular cuboid-shaped crystalline structure, consistent with the literature [30,38]. The ceph@MOF-5 images showed an irregular clustered shape appearing more amorphous and flaked. This also agrees with the slightly broader PXRD peaks for ceph@MOF-5, as shown in Figure 1.

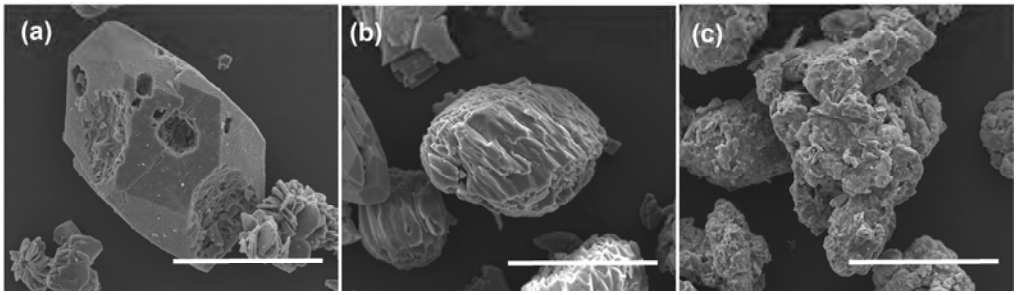

Figure 2. SEM images of (**a**) pristine MOF-5, (**b**) met@MOF-5 and (**c**) ceph@MOF-5 are shown. The scale bar is 200 μm.

The SEM imaging of the polymer composites, which is presented in Figure 3, shows the scattered microcrystalline crystals of the MOFs within the polymer matrix. The elemental mapping of the polymer composites (Figure S5) confirmed the presence of Zn, which was well distributed, confirming the presence of loaded ceph@MOF-5 in PCL-ceph@MOF-5 and PLGA-ceph@MOF-5 [45].

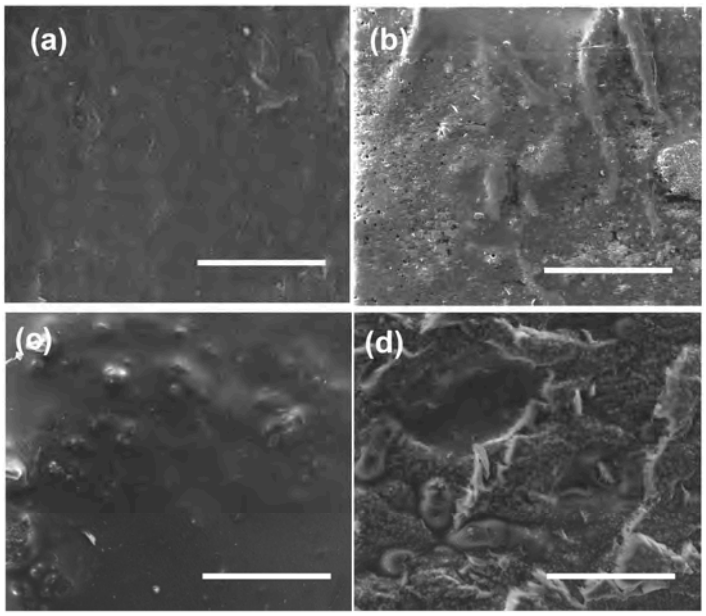

Figure 3. SEM images of (**a**) PCL-ceph@MOF-5; the scale bar is 50 μm. (**b**) PCL-met@MOF-5; the scale bar is 1 mm. (**c**) PLGA-ceph@MOF-5; (**d**) PLGA-met@MOF-5.

3.3. FT-IR

The successful encapsulation of the drugs into the MOFs and composite materials was further examined by comparing their IR-spectra (Figure 4). The spectra for the pristine MOF-5 were consistent with literature, [30] with its absorption band centred at a region of 2932 cm^{-1} because of the C-H aromatic bond stretching vibration. Two other strong bands were evident at 1656 cm^{-1} and 1595 cm^{-1}, which is attributed to C=O and C-C stretching vibration due to the presence of the skeletal vibration of the aromatic ring found in the linker 1,4–benzene dicarboxylic acid. Another band is observed at 1378 cm^{-1} due to the C-H stretching vibration, while minor bands found between 822 cm^{-1} and 1153 cm^{-1} are also assigned to the O–C=O symmetric and asymmetric stretching vibrations; also, the C–O stretching vibration found in the unreacted 1,4 benzene dicarboxylic acid contributes to these minor bands as well. The remaining absorption bands between 660 cm^{-1} and 822 cm^{-1} occur because of the stretching vibrations of the aromatic ring [46].

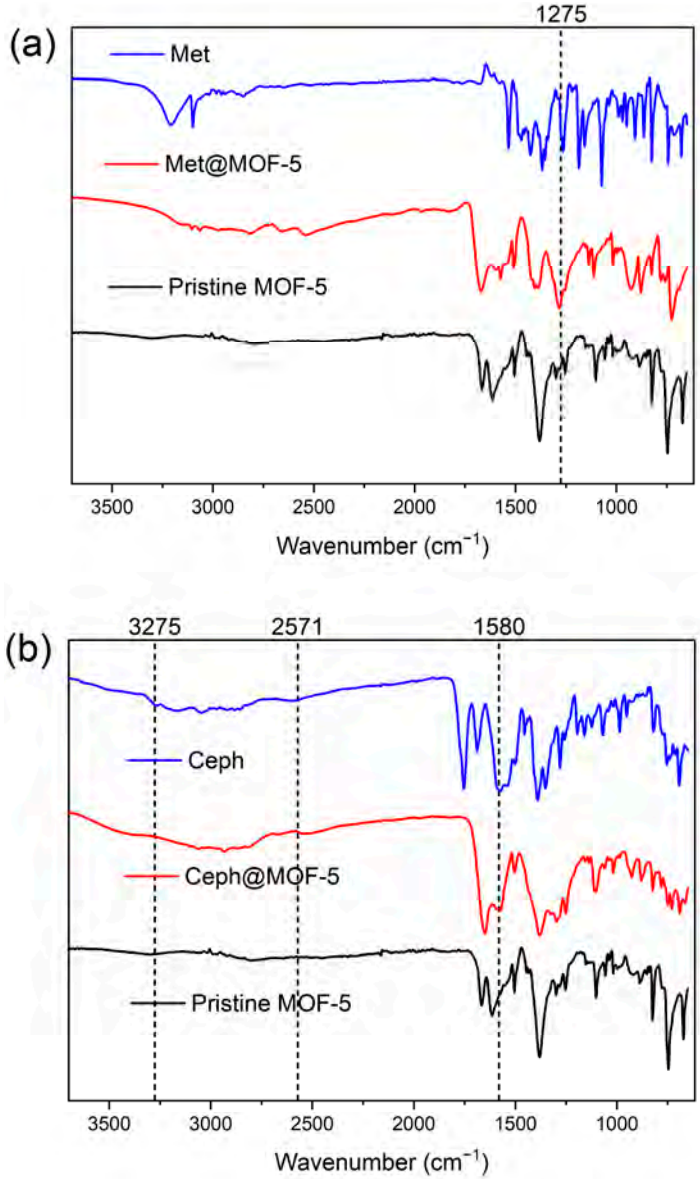

Figure 4. FT-IR spectra for Met, met@MOF-5 and pristine MOF-5 compared (**a**) with the characteristic peak of Met found between 1232 cm^{-1} and 1404 cm^{-1} of the met@MOF-5 spectra. IR spectra of Ceph, ceph@MOF-5 and pristine MOF-5 (**b**), with the characteristic peak of Ceph present at 1504 cm^{-1}, confirming the presence of the drugs in their respective samples.

In the case of Met, the stretching of the CH_3 functional group was shown at 2954 cm^{-1} and 2897 cm^{-1} [47]. The spectra of the met@MOF-5 showed characteristic peaks of the Met at 1600 cm^{-1} and at 1523 cm^{-1}, where additional peaks were observed because of the C=C and C=N stretching, whilst the N=O asymmetry accounted for the peaks at 1479 cm^{-1}. Extra peaks found from 1275 cm^{-1} to 1096 cm^{-1}, at 1070 cm^{-1} and 711 cm^{-1}, occurred due to C–O stretching, C–N stretching and C–H bending. This shows that the drug had been successfully loaded, while the absorption band found at 2935 cm^{-1} is present due to the stretching of the O–H bond. The spectra of ceph@MOF-5 also showed that the characteristic peaks of the Ceph drug at 3275 cm^{-1} due to the N–H bond present, from 1680 cm^{-1} to 1760 cm^{-1}, was because of the C=O, whilst additional peaks from 2550 cm^{-1} to 2620 cm^{-1} were due to the S-H. The C–N bond accounted for the peaks from 1020 cm^{-1} to 1220 cm^{-1}, and those found from 1000 cm^{-1} to 1300 cm^{-1} were because of the C-O bond. This indicates the presence of the Ceph drug molecules, and this is in agreement with the XRD patterns

and SEM images shown above, which all suggest the successful incorporation of the drug molecules into the pores of the loaded MOF-5.

The FT-IR analysis conducted on the polymer composites showed the characteristic peaks of the loaded drug molecules, as depicted in Figure 5. It was observed that comparing the IR spectra of PLGA-ceph@MOF-5 with the spectra of the pristine PLGA, the peak found at 1571 cm^{-1} was intensified after the loading. Another major characteristic peak found at 1376 cm^{-1} was observed to have intensified after loading due to the symmetric stretched vibration of COO and the bending vibration of the hydrogen bond amongst the NH groups of the Ceph molecule, and this suggests the presence of the Ceph drug molecules due to the incorporation of the loaded MOF-5 into the PLGA-ceph@MOF-5. This same peak was found in both ceph@MOF-5 and PCL-ceph@MOF-5, as shown above. The absorption bands found at 1105 cm^{-1} and 3000 cm^{-1} were also observed to have reduced after incorporation due to the C–H bonds of the Ceph molecule [45]. For both PLGA-met@MOF-5 and PCL-met@MOF-5, the characteristic peak of the Met drug molecule present with small shifting at 3210 cm^{-1} and 1536 cm^{-1} can be attributed to the O-H stretching due to the hydrogen bonding and the N=O asymmetrical stretching, respectively [47].

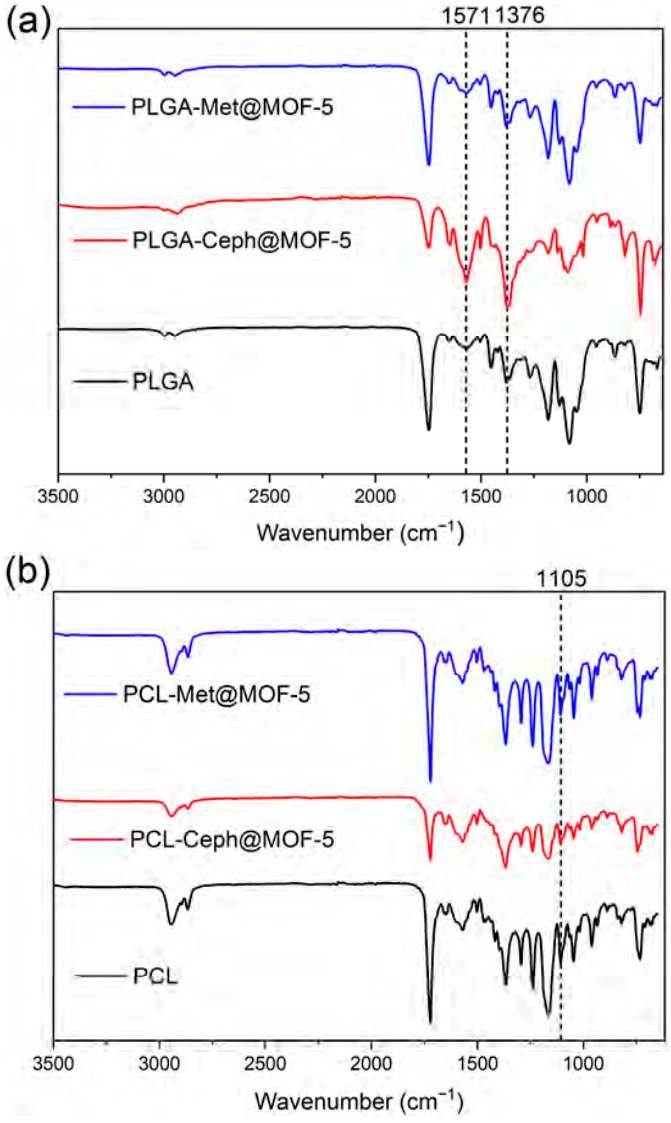

Figure 5. FT-IR spectra of pristine PCL, PCL-met@MOF-5 and PCL-ceph@MOF-5 (**a**) and IR spectra of PLGA, PLGA-met@MOF-5 and PLGA-ceph@MOF-5 (**b**) are shown.

3.4. TGA

Based on the successful incorporation of the drugs, as suggested by the previous characterisation results, the thermal stability of the pristine MOF-5 was compared with the thermal behaviour of the loaded ceph@MOF-5 and met@MOF-5 (Figure 6). The TGA plots of the loaded polymers give information on the weight loss changes with increasing temperatures, due to the presence of antibiotics and composite materials, as displayed in their respective TGA plots below.

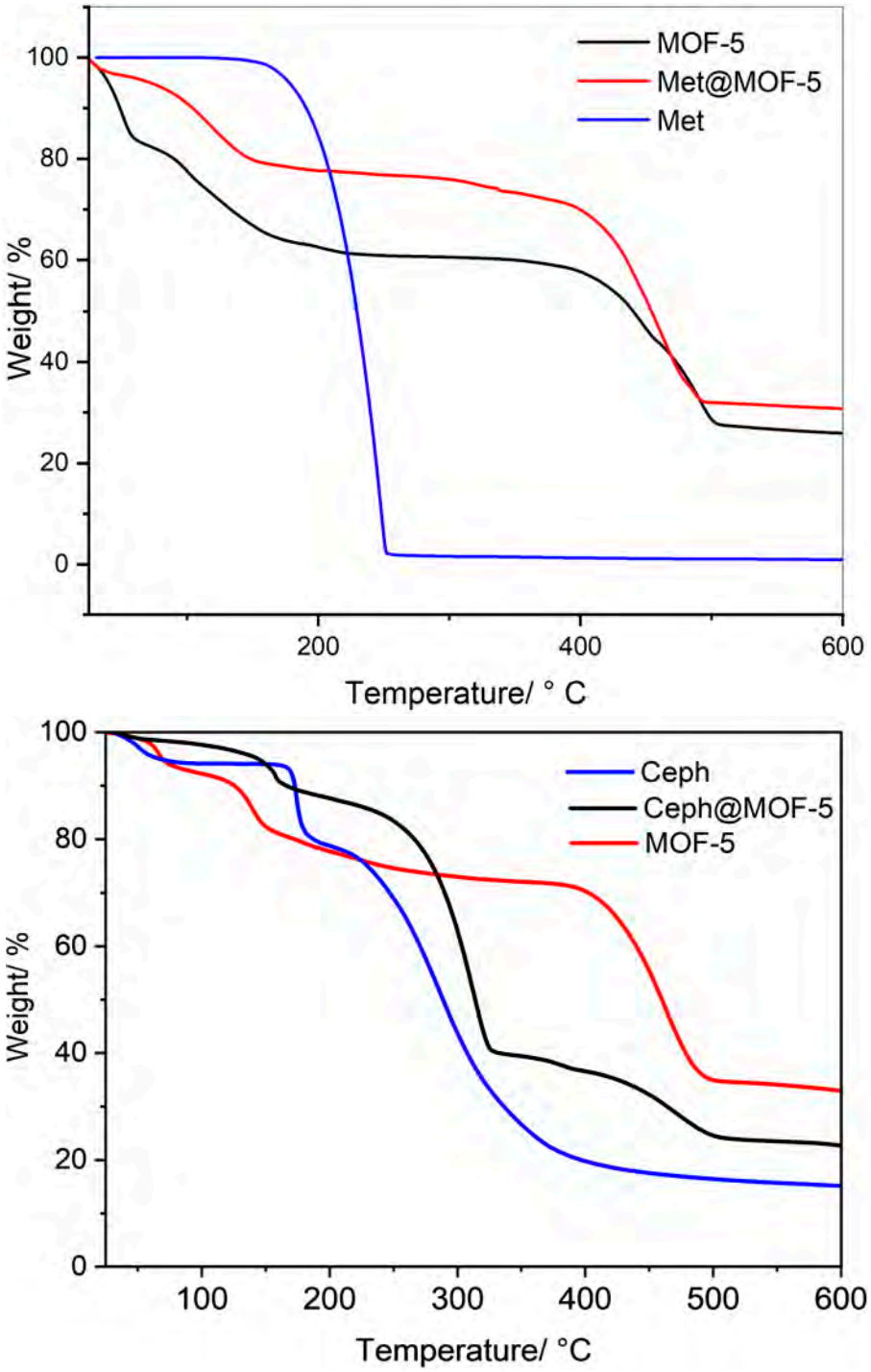

Figure 6. TGA plots of met@MOF-5, Met and pristine MOF-5 (**top**). Ceph, ceph@MOF-5 and pristine MOF-5 (**bottom**) are shown.

As expected, the TGA plots of the pristine MOF-5 indicated four distinct weight losses [27]: between 52 °C and 82.5 °C (5%) due to the removal of water molecules; between 82.5 °C and 175 °C (10%) due to the removal of DMF molecules; the third weight loss was assigned to the partial degradation of the MOF-5 framework, between 175 °C and 412 °C (12%), while between 412 °C and 500 °C (42%) indicated the final weight loss due to the full degradation of the MOF-5 framework at that point [46,47]. For the met@MOF-5 crystals, the TGA plots showed no weight loss until 150 °C; the first loss was then between 150 °C and 178 °C (13%), and due to the loss of DMF molecules, the second weight loss occurred between 178 °C and 325 °C (25%) due to the degradation of the Met drug molecules, which is observed to have its degrading temperature of 180 °C, within this temperature range. This suggests that the drug was successfully loaded and present in the pores of the MOF-5. The total disintegration of the framework then occurs between 450 °C and 510 °C (32%) after which it remains constant until 600 °C. In the case of ceph@MOF-5 crystals, three major weight losses were observed. The first drop is from 50 °C to 173 °C (8%), which can be accounted for by the loss of water and DFM molecules; another major drop is observed between 175 °C and 327 °C (52%) due to degradation of the Ceph drug molecules. Compared to the TGA plots of Ceph, they have a similar degrading temperature range suggesting the presence of the Ceph molecules after successful incorporation. Then, another drop in weight from 327 °C to 500 °C (15%) was observed due to the breakdown of the MOF framework, and it remained constant until 600 °C.

The TGA plots of the polymer composites are also illustrated in Figure 7, from which it was observed that for the PCL-met@MOF-5 and PLGA-met@MOF-5 composites, the polymers began to degrade at approximately 180 °C, which is noted to be the degrading temperature of Met from Figure 6 and confirms the presence of the loaded MOF in the composites [48].

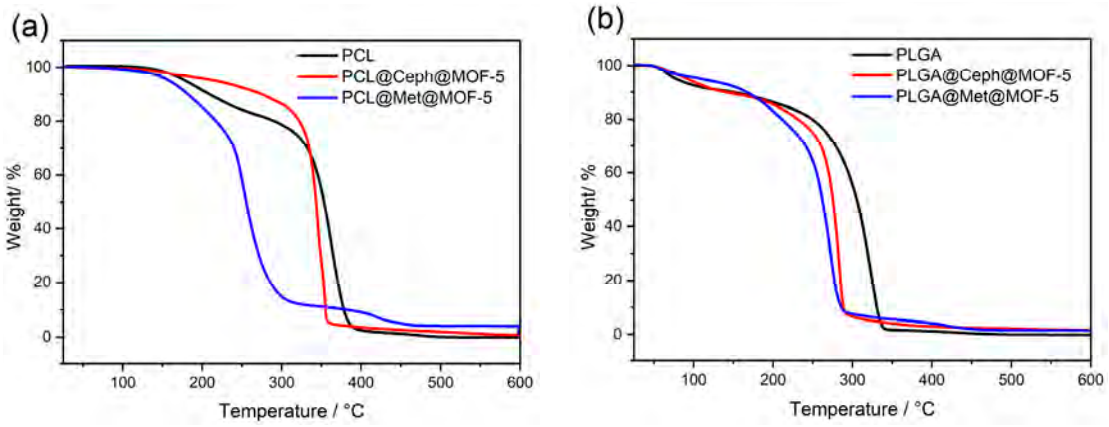

Figure 7. TGA plots of PCL, PCL-met@MOF-5 and PCL-ceph@MOF-5 compared, (**a**) and plots of PLGA, PLGA-met@MOF-5 and PLGA-ceph@MOF-5 (**b**).

In the case of PCL-ceph@MOF-5 and PLGA-ceph@MOF-5, the major degradation began at approximately 300 °C, which accounts for the degradation of ceph@MOF-5, as depicted in Figure 6 above, and this confirms the successful encapsulation of the loaded MOF into the polymer composites.

3.5. Drug Release Profile

From the drug release data illustrated in Figure 8, it can be observed that the release of Met (a) is slightly higher than that of Ceph (b). This can be attributed to the relatively smaller molecular size of Met ($C_6H_9N_3O_3$) than Ceph ($C_{16}H_{17}N_3O_4S$), which enables Met to penetrate through the small pore of MOF-5 easily leading to a higher loading and release rate [49].

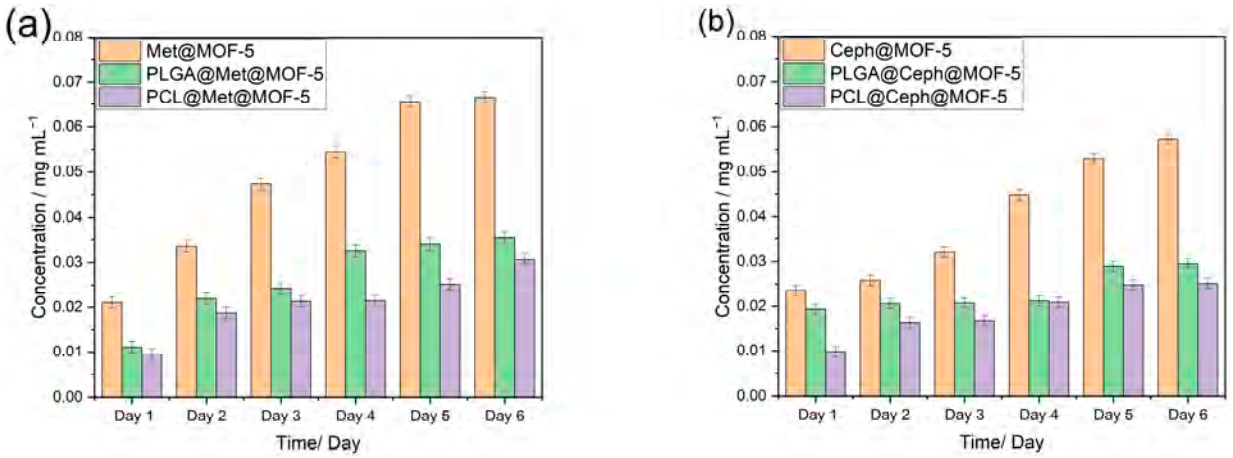

Figure 8. Release studies of drug-loaded MOFs and composites over 6 days for (**a**) met@MOF-5, PLGA@met@MOF-5 and PCL@met@MOF-5. (**b**) ceph@MOF-5, PLGA@ceph@MOF-5 and PCL@ceph@MOF-5.

It is also evident from the data that across all six days of the study, PLGA-met@MOF-5 produced the release of lower concentrations than in met@MOF-5 alone, which comparatively releases drugs faster and in higher concentrations. This is assigned to the fact that the PLGA-met@MOF-5 composite will have to undergo the degradation of the PLGA polymer before the incorporated MOF-5 will also begin to break down for the release of the Met drug molecules [50]. In addition, as confirmed by the XRD patterns shown in Figure 1 above, the amorphous structure of met@MOF-5 results in the drug molecules being loosely held and not captured deep into the crystal lattice of the MOF-5, hence the release of the drugs in higher concentrations [31,51]. Similar observations can be noted for PLGA-ceph@MOF-5, as it also provides releases of lower concentrations than releases from ceph@MOF-5 for the same reasons stated above. It can therefore be deduced that the drug-release rate from the loaded polymer composites as compared to the release rate from the loaded MOF-5 is slower, more gradual and more sustained over the six-day period of the study.

It was also observed that the release from loaded PLGA-MOF composites was in relatively higher concentrations compared to PCL-MOF composites. For example, PLGA-met@MOF-5 drug release had a concentration of 0.025 mg mL^{-1} compared to 0.02 mg mL^{-1} for PCL- met@MOF-5, an observation similar to that of PLGA-ceph@MOF-5 compared with PCL-ceph@MOF-5. This observation is assigned to the fact that PCL belongs to the class of slow-degrading polymers [52] that take longer to degrade and enhance the release of the drug molecules loaded into the polymer matrix, resulting in the subsequent release of drugs in lower concentrations, especially under physiological conditions, which is isotonic to the PBS release medium used in this study [53].

PLGA is an amorphous polymer, while PCL is a semi-crystalline polymer [51], and the morphologies are shown in Figure 3. The amorphous nature of PLGA is possibly responsible for the loosely held loaded MOF particles leading to quicker drug release than in PCL [54]. The hydrophobicity of PLGA may also contribute positively to the release in higher concentrations [54]. Earlier studies demonstrated the use of PCL-loaded composites for a rather long term prolonged drug delivery [54], while other studies reported the use of PLGA-loaded composites for a comparatively shorter term of release [26]. This work agrees with these previously reported studies, as the data suggest the slower release rate of drugs from the PCL-loaded composites compared to PLGA, and the concentrations from the release are significant enough to inhibit the growth of the various bacterial strains that were studied, as shown in the next Section 3.6.

From the release studies, it can be inferred that the concentrations exceed the limit needed for the effective inhibition of clinically relevant, infection-causing pathogens. For example, the minimum inhibitory concentration (MIC) of cephalexin required to treat methicillin-sensitive *Staphylococcus aureus* (MSSA) infections is 2 μg mL^{-1} [55]. For Met,

an effective MIC against many anaerobic bacterial strains ranges between 0.125 μg mL^{-1} and 1 μg mL^{-1} indicating the potential application of these composites for biomedical applications, such as in developing antimicrobial gauze and disinfectant surfaces [11,56,57].

Previous studies by Kumar et al. have reported a maximum loading capacity of 539.33 mg g^{-1} for metronidazole in MOF-5 at pH 2 [58]. Other materials, like chitosan/graphene composites, were also explored for the controlled delivery of metronidazole, demonstrating prolonged release over 3.5 days [59]. The drug release profile of cephalexin using MIL-101 nanocomposites was also studied, showing pH-responsive drug release [60]. Other studies have incorporated cephalexin into PLA:PVA/HAP:TiO_2 biocompatible scaffolds for bone regeneration [61].

In this study, the prolonged release of metronidazole and cephalexin was studied for 6 days using MOF-5 and PCL-MOF-5 composites, showing the release of effective concentrations for practical applications.

3.6. Antimicrobial Studies

Following the confirmation of the presence of the drug molecules in the loaded MOFs using the above techniques, the antimicrobial properties of the loaded MOFs and their corresponding polymer–MOF composites were tested against Gram-positive and Gram-negative bacteria, using the inhibition zone assay (Figure 9) against the four selected bacterial strains. The zones of inhibition of pristine MOFs and polymers only are presented in Table 1, those of pure Met, Met-loaded MOFs and polymer composites are in Table 2 and those of pure Ceph, Ceph-loaded MOFs and polymer composites are in Table 3.

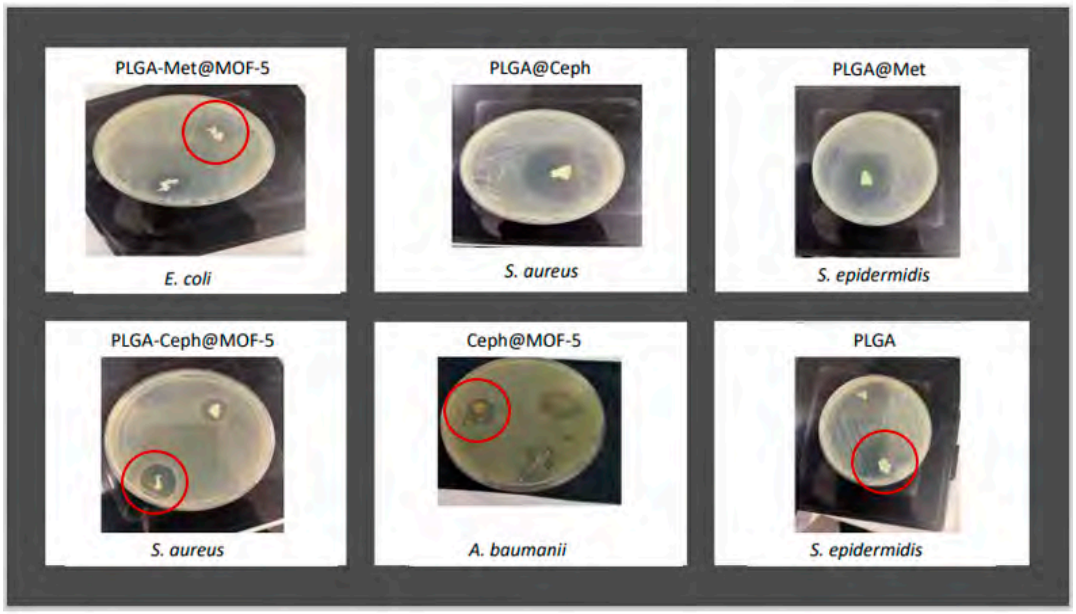

Figure 9. Images of the zones of inhibition on agar plates after microbial testing of the loaded composites against the strains of bacteria. The relevant areas are circulated where multiple tests were performed.

Table 1. Zones of inhibition of pristine MOF, PLGA and PCL against four bacterial strains.

	Inhibition Zone (mm)			
	S. epidermidis	***S. aureus***	***E. coli***	***A. baumanii***
Pristine MOF-5	26 ± 1.5	28 ± 0	13 ± 1.1	13 ± 0.5
PLGA	51 ± 1.5	-	-	-
PCL	-	-	-	-

Table 2. Zones of inhibition of Met, Met-loaded MOF and polymer composites against four bacterial strains.

	Inhibition Zone (mm)			
	S. epidermidis	***S. aureus***	***E. coli***	***A. baumanii***
Met	23 ± 0.5	20 ± 0.5	13 ± 0.5	18 ± 0.5
met@MOF-5	21 ± 0.5	15 ± 0	10 ± 0	10 ± 0
met@PLGA	43 ± 1	-	-	-
met@PCL	5 ± 1	-	-	-
MOF-5@PLGA	73 ± 1.5	83 ± 0	-	-
MOF5@PCL				
PLGA-met@MOF-5	-	-	-	-
PCL-met@MOF-5				

Table 3. Zones of inhibition of Ceph, Ceph-loaded MOF and polymer composites against four bacterial strains.

	Inhibition Zone (mm)			
	S. epidermidis	***S. aureus***	***E. coli***	***A. baumanii***
Ceph	79 ± 1	66 ± 1	34 ± 0.5	-
ceph@MOF-5	34 ± 0.5	31 ± 1.5	10 ± 0	13 ± 0.5
ceph@PLGA	73 ± 0.5	42 ± 0.5	25 ± 1	-
ceph@PCL	16 ± 0	32 ± 0.5	16 ± 0	-
PLGA-ceph@MOF-5	75 ± 0	7 ± 0	-	-
PCL-ceph@MOF-5	6 ± 0.5	11 ± 1	-	-

The susceptibility of the bacterial strains to the pure drugs was first assessed. Ceph is widely used against Gram-positive bacteria, more than against Gram-negative bacteria, and this agrees with the zones of inhibition recorded in Table 3 below. The growth of *S. epidermidis* and *S. aureus* was largely inhibited by Ceph more than in the case of Gram-negative bacteria, *E. coli* and *A. baumanii* [62,63]. It was observed that *A. baumanii* was not susceptible to Ceph, which is consistent with literature and previous studies that report the extreme resistance of this bacterial strain to cephalosporins [64]. Compared to the antimicrobial strength of Met, which is a first-class antibiotic, well-known for a relatively stronger antimicrobial reaction against both Gram-negative and Gram-positive bacteria [65], Met inhibited all bacterial strains, as shown below (Table 2). The pristine PLGA and PCL were also tested as controls, and there was no inhibition across all bacterial strains, apart from the PLGA that presented a large zone of inhibition against *S. epidermidis* (Table 1). This is however expected and can be attributed to the antimicrobial properties of the glycolic and lactic acid composition of PLGA and the very high susceptibility of the Gram-positive *S. epidermidis* [66–68].

From Table 2, met@MOF-5 inhibited the growth of Gram-positive bacteria, *S. aureus* and *S. epidermidis*, more than the Gram-negative bacteria, *E. coli* and *A. baumanii*, and this is attributed to the strong resistance of Gram-negative bacteria to Met [69]. In the case of PLGA-met@MOF-5, it was observed that the zones of inhibition significantly decreased, with no inhibition against the resistant Gram-negative bacteria; however, the susceptible *S. epidermidis* was largely inhibited [70], and this can be assigned to the slow release of drug molecules due to the degradability of the composite and the MOF before the release of the drug molecules. Compared with PCL-met@MOF-5, there was no inhibition against all strains of bacteria. This agrees with the data from the drug release studies displayed in Figure 8 above, which depicts the slower release of drugs from PCL composites in relatively lower concentrations. This is because PCL has a slower degradation rate and takes much longer to release the loaded MOFs carrying the drug molecules [52]. Ceph@MOF-5 reacted better against the Gram-positive bacteria than the resistant Gram-negative bacteria strains owing to the presence of the Ceph drug molecules, which is consistent with the findings of

previous studies [63]. However, in relation to the polymer composites, PLGA-ceph@MOF-5 inhibited bacterial growth better than PCL-ceph@MOF-5 for same reasons that were discussed above.

Additionally, the drugs and MOF (without being loaded) were incorporated together into both polymers and tested against the bacterial strains. The measured zones of inhibition were all larger than those of their corresponding composites with MOFs loaded with drugs (Figure 9 and Tables 1–3). This is attributed to the immediate release of the MOF and drug molecules from the polymer composite immediately after degradation relative to the gradual release of drug molecules as a result of degradation of the polymer and MOF in the case of loaded MOFs incorporated into polymers. This confirms that the release of the drug molecules from the loaded MOFs incorporated into the loaded polymers was relatively gradual and released at a slower controlled rate, and this was the main aim of this study.

4. Conclusions

In this study, the biocompatible Zn-based MOF-5 was loaded post-synthetically with two antimicrobials, Ceph and Met, respectively. The pristine MOF-5, drug-loaded MOF-5 and loaded polymer composites were characterised to confirm that the MOFs were successfully synthesised and loaded with the drugs using efficient methodologies. The loaded MOF-5 was incorporated into two biodegradable polymers, PLGA and PCL, and the release of the drug from the polymer composite and pores of the MOF-5 was studied. PCL-ceph@MOF-5 demonstrated the most gradual and extended-release profile. In a descending order, this was followed by PCL-met@MOF-5, PLGA-ceph@MOF-5 and PLGA-met@MOF-5. The steady rise in the drug concentration of PCL-ceph@MOF-5 and PCL-met@MOF-5 over the six-day study period provides a more extended sustained release, which is an advantage over the PLGA comparatively, achieving the main objectives of this study. That notwithstanding, further studies are ongoing, which seek to use the PCL-ceph@MOF-5 and PCL-met@MOF-5 composites in medical devices, such as patches, to provide the extended release of incorporated drugs. This study has successfully brought out a comparative analysis for the provision of the more efficient and sustained delivery of Ceph and Met antimicrobials, as stipulated in our initial objectives, and this can be a potential tool to control the rise in antimicrobial resistance by providing a means of sustained localised applications.

Supplementary Materials: The following supporting information can be downloaded at: https://www.mdpi.com/article/10.3390/app131910611/s1, Figure S1: Calibration curve for cephalexin; Figure S2: Calibration curve for cephalexin; Figure S3: Lambda max for metronidazole; Figure S4: Lambda max for cephalexin; Figure S5: EDS analysis of MOF-polymer composites; Figure S6: PXRD of the drug-loaded MOF composites before and after exposure to PBS for 24 h: (A) PCL composites (B) PLGA composites.

Author Contributions: A.A., execution of concept and idea, experiments, characterisation of materials, data collection, data analysis and manuscript preparation; L.A.M.M., manuscript preparation, data analysis, illustration of figures and Supporting Information; M.G.K., supervision and data analysis, review and editing of manuscript; A.L.K., supervision and data analysis, review and editing of manuscript; S.N., supervision, conceptualisation, data analysis and manuscript preparation. All authors have read and agreed to the published version of the manuscript.

Funding: This research received no external funding.

Institutional Review Board Statement: Not applicable.

Informed Consent Statement: Not applicable.

Data Availability Statement: Data can be available on request from the authors.

Acknowledgments: A.A. acknowledges a scholarship from the Ghana Scholarship Secretariat, Accra-Ghana. L.A.M.M. acknowledges an Erasmus exchange studentship.

Conflicts of Interest: The authors declare no conflict of interest.

References

1. Abushaheen, M.A.; Muzaheed; Fatani, A.J.; Alosaimi, M.; Mansy, W.; George, M.; Acharya, S.; Rathod, S.; Divakar, D.D.; Jhugroo, C.; et al. Antimicrobial resistance, mechanisms and its clinical significance. *Dis. Mon.* **2020**, *66*, 100971. [CrossRef] [PubMed]
2. de Kraker, M.E.A.; Stewardson, A.J.; Harbarth, S. Will 10 Million People Die a Year due to Antimicrobial Resistance by 2050? *PLoS Med.* **2016**, *13*, e1002184. [CrossRef] [PubMed]
3. Seil, J.T.; Webster, T.J. Antimicrobial applications of nanotechnology: Methods and literature. *Int. J. Nanomed.* **2012**, *7*, 2767–2781. [CrossRef]
4. Lu, X.; Ye, J.; Zhang, D.; Xie, R.; Bogale, R.F.; Sun, Y.; Zhao, L.; Zhao, Q.; Ning, G. Silver carboxylate metal–organic frameworks with highly antibacterial activity and biocompatibility. *J. Inorg. Biochem.* **2014**, *138*, 114–121. [CrossRef] [PubMed]
5. Sava Gallis, D.F.; Butler, K.S.; Agola, J.O.; Pearce, C.J.; McBride, A.A. Antibacterial Countermeasures via Metal–Organic Framework-Supported Sustained Therapeutic Release. *ACS Appl. Mater.* **2019**, *11*, 7782–7791. [CrossRef] [PubMed]
6. Rojas, S.; Wheatley, P.S.; Quartapelle-Procopio, E.; Gil, B.; Marszalek, B.; Morris, R.E.; Barea, E. Metal–organic frameworks as potential multi-carriers of drugs. *CrystEngComm* **2013**, *15*, 9364–9367. [CrossRef]
7. Rojas, S.; Quartapelle-Procopio, E.; Carmona, F.J.; Romero, M.A.; Navarro, J.A.R.; Barea, E. Biophysical characterisation, antitumor activity and MOF encapsulation of a half-sandwich ruthenium(ii) mitoxantronato system. *J. Mater. Chem. B* **2014**, *2*, 2473–2477. [CrossRef]
8. Sun, T.; Zhang, Y.S.; Pang, B.; Hyun, D.C.; Yang, M.; Xia, Y. Engineered Nanoparticles for Drug Delivery in Cancer Therapy. *Angew. Chem. Int. Ed.* **2014**, *53*, 12320–12364. [CrossRef]
9. Abdelaziz, H.M.; Gaber, M.; Abd-Elwakil, M.M.; Mabrouk, M.T.; Elgohary, M.M.; Kamel, N.M.; Kabary, D.M.; Freag, M.S.; Samaha, M.W.; Mortada, S.M.; et al. Inhalable particulate drug delivery systems for lung cancer therapy: Nanoparticles, microparticles, nanocomposites and nanoaggregates. *J. Control Release* **2018**, *269*, 374–392. [CrossRef]
10. Wuttke, S.; Lismont, M.; Escudero, A.; Rungtaweevoranit, B.; Parak, W.J. Positioning metal-organic framework nanoparticles within the context of drug delivery—A comparison with mesoporous silica nanoparticles and dendrimers. *Biomaterials* **2017**, *123*, 172–183. [CrossRef]
11. Livesey, T.C.; Mahmoud, L.A.M.; Katsikogianni, M.G.; Nayak, S. Metal–Organic Frameworks and Their Biodegradable Composites for Controlled Delivery of Antimicrobial Drugs. *Pharmaceutics* **2023**, *15*, 274. [PubMed]
12. Mallakpour, S.; Nikkhoo, E.; Hussain, C.M. Application of MOF materials as drug delivery systems for cancer therapy and dermal treatment. *Coord. Chem. Rev.* **2022**, *451*, 214262. [CrossRef]
13. Batten, S.R.; Champness, N.R.; Chen, X.-M.; Garcia-Martinez, J.; Kitagawa, S.; Öhrström, L.; O'Keeffe, M.; Suh, M.P.; Reedijk, J. Terminology of metal–organic frameworks and coordination polymers (IUPAC Recommendations 2013). *Pure Appl. Chem.* **2013**, *85*, 1715–1724. [CrossRef]
14. Cui, Y.; Yue, Y.; Qian, G.; Chen, B. Luminescent Functional Metal–Organic Frameworks. *Chem. Rev.* **2012**, *112*, 1126–1162. [CrossRef]
15. Zheng, H.; Zhang, Y.; Liu, L.; Wan, W.; Guo, P.; Nyström, A.M.; Zou, X. One-pot Synthesis of Metal–Organic Frameworks with Encapsulated Target Molecules and Their Applications for Controlled Drug Delivery. *J. Am. Chem. Soc.* **2016**, *138*, 962–968. [CrossRef]
16. Chen, S.; Lu, J.; You, T.; Sun, D. Metal-organic frameworks for improving wound healing. *Coord. Chem. Rev.* **2021**, *439*, 213929. [CrossRef]
17. Xie, J.; Wang, Y.; Liu, W.; Yin, X.; Chen, L.; Zou, Y.; Diwu, J.; Chai, Z.; Albrecht-Schmitt, T.E.; Liu, G.; et al. Highly Sensitive Detection of Ionizing Radiations by a Photoluminescent Uranyl Organic Framework. *Angew. Chem. Int. Ed.* **2017**, *56*, 7500–7504. [CrossRef] [PubMed]
18. Wang, C.; Liu, X.; Chen, J.P.; Li, K. Superior removal of arsenic from water with zirconium metal-organic framework UiO-66. *Sci. Rep.* **2015**, *5*, 16613. [CrossRef]
19. Rocha, J.; Carlos, L.D.; Paz, F.A.A.; Ananias, D. Luminescent multifunctional lanthanides-based metal-organic frameworks. *Chem. Soc. Rev.* **2011**, *40*, 926–940. [CrossRef]
20. Nandi, S.; Singh, S.K.; Mullangi, D.; Illathvalappil, R.; George, L.; Vinod, C.P.; Kurungot, S.; Vaidhyanathan, R. Low Band Gap Benzimidazole COF Supported Ni3N as Highly Active OER Catalyst. *Adv. Energy Mater.* **2016**, *6*, 1601189. [CrossRef]
21. Mullangi, D.; Chakraborty, D.; Pradeep, A.; Koshti, V.; Vinod, C.P.; Panja, S.; Nair, S.; Vaidhyanathan, R. Highly Stable COF-Supported Co/$Co(OH)_2$ Nanoparticles Heterogeneous Catalyst for Reduction of Nitrile/Nitro Compounds under Mild Conditions. *Small* **2018**, *14*, 1801233. [CrossRef] [PubMed]
22. Mullangi, D.; Dhavale, V.; Shalini, S.; Nandi, S.; Collins, S.; Woo, T.; Kurungot, S.; Vaidhyanathan, R. Low-Overpotential Electrocatalytic Water Splitting with Noble-Metal-Free Nanoparticles Supported in a sp3 N-Rich Flexible COF. *Adv. Energy Mater.* **2016**, *6*, 1600110. [CrossRef]
23. Aden, S.F.; Mahmoud, L.A.M.; Ivanovska, E.H.; Terry, L.R.; Ting, V.P.; Katsikogianni, M.G.; Nayak, S. Controlled delivery of ciprofloxacin using zirconium-based MOFs and poly-caprolactone composites. *J. Drug Deliv. Sci. Technol.* **2023**, *88*, 104894. [CrossRef]
24. Aguado, S.; Quirós, J.; Canivet, J.; Farrusseng, D.; Boltes, K.; Rosal, R. Antimicrobial activity of cobalt imidazolate metal–organic frameworks. *Chemosphere* **2014**, *113*, 188–192. [CrossRef] [PubMed]

25. Nabipour, H.; Sadr, M.H.; Bardajee, G.R. Synthesis and characterization of nanoscale zeolitic imidazolate frameworks with ciprofloxacin and their applications as antimicrobial agents. *New J. Chem.* **2017**, *41*, 7364–7737. [CrossRef]
26. Tenover, F.C. Mechanisms of antimicrobial resistance in bacteria. *Am. J. Infect. Control* **2006**, *34*, S3. [CrossRef]
27. Cai, W.; Wang, J.; Chu, C.; Chen, W.; Wu, C.; Liu, G. Metal–Organic Framework-Based Stimuli-Responsive Systems for Drug Delivery. *Adv. Sci.* **2019**, *6*, 1801526. [CrossRef]
28. Murphy, M.; Ting, K.; Zhang, X.; Soo, C.; Zheng, Z. Current Development of Silver Nanoparticle Preparation, Investigation, and Application in the Field of Medicine. *J. Nanomater.* **2015**, *2015*, 696918. [CrossRef]
29. McKinlay, A.C.; Morris, R.E.; Horcajada, P.; Férey, G.; Gref, R.; Couvreur, P.; Serre, C. BioMOFs: Metal-Organic Frameworks for Biological and Medical Applications. *Angew. Chem. Int. Ed.* **2010**, *49*, 6260–6266. [CrossRef]
30. Li, H.; Eddaoudi, M.; O'Keeffe, M.; Yaghi, O.M. Design and synthesis of an exceptionally stable and highly porous metal-organic framework. *Nature* **1999**, *402*, 276. [CrossRef]
31. Mahmoud, L.A.M.; Telford, R.; Livesey, T.C.; Katsikogianni, M.; Kelly, A.L.; Terry, L.R.; Ting, V.P.; Nayak, S. Zirconium-Based MOFs and Their Biodegradable Polymer Composites for Controlled and Sustainable Delivery of Herbicides. *ACS Appl. Bio Mater.* **2022**, *5*, 3972–3981. [CrossRef] [PubMed]
32. Lan, A.; Li, K.; Wu, H.; Olson, D.H.; Emge, T.J.; Ki, W.; Hong, M.; Li, J. Luminescent Microporous Metal-Organic Framework for the Fast and Reversible Detection of High Explosives. *Angew. Chem. Int. Ed.* **2009**, *48*, 2334–2338. [CrossRef] [PubMed]
33. Dwivedi, R.; Kumar, S.; Pandey, R.; Mahajan, A.; Nandana, D.; Katti, D.S.; Mehrotra, D. Polycaprolactone as biomaterial for bone scaffolds: Review of literature. *J. Oral. Biol. Craniofac Res.* **2020**, *10*, 381–388. [CrossRef]
34. Christen, M.-O.; Vercesi, F. Polycaprolactone: How a Well-Known and Futuristic Polymer Has Become an Innovative Collagen-Stimulator in Esthetics. *Clin. Cosmet. Investig. Dermatol.* **2020**, *13*, 31–48. [CrossRef] [PubMed]
35. Jiang, W.; Gupta, R.K.; Deshpande, M.C.; Schwendeman, S.P. Biodegradable poly(lactic-co-glycolic acid) microparticles for injectable delivery of vaccine antigens. *Adv. Drug Deliv. Rev.* **2005**, *57*, 391–410. [CrossRef]
36. Dziadek, M.; Dziadek, K.; Checinska, K.; Salagierski, S.; Choinska, E.; Szatkowski, P.; Wajda, A.; Kopec, A.; Cholewa-Kowalska, K. Polyphenolic compounds affect the long-term degradation behaviour of polymer and composite materials based on PCL, PLGA, and bioactive glass. *Sustain. Mater. Technol.* **2023**, *35*, e00568. [CrossRef]
37. Engelberg, I.; Kohn, J. Physico-mechanical properties of degradable polymers used in medical applications: A comparative study. *Biomaterials* **1991**, *12*, 292–304. [CrossRef]
38. Kumar, G.; Masram, D.T. Sustainable Synthesis of MOF-5@GO Nanocomposites for Efficient Removal of Rhodamine B from Water. *ACS Omega* **2021**, *6*, 9587–9599. [CrossRef]
39. Baptista, P.V.; McCusker, M.P.; Carvalho, A.; Ferreira, D.A.; Mohan, N.M.; Martins, M.; Fernandes, A.R. Nano-Strategies to Fight Multidrug Resistant Bacteria-"A Battle of the Titans". *Front. Microbiol.* **2018**, *9*, 1441. [CrossRef]
40. Zapata, A.; Ramirez-Arcos, S. A Comparative Study of McFarland Turbidity Standards and the Densimat Photometer to Determine Bacterial Cell Density. *Curr. Microbiol.* **2015**, *70*, 907–909. [CrossRef]
41. Hafizovic, J.; Bjørgen, M.; Olsbye, U.; Dietzel, P.D.C.; Bordiga, S.; Prestipino, C.; Lamberti, C.; Lillerud, K.P. The Inconsistency in Adsorption Properties and Powder XRD Data of MOF-5 Is Rationalized by Framework Interpenetration and the Presence of Organic and Inorganic Species in the Nanocavities. *J. Am. Chem. Soc.* **2007**, *129*, 3612–3620. [CrossRef] [PubMed]
42. Colin McKinstry, C.; Cathcart, R.J.; Cussen, E.J.; Fletcher, A.J.; Patwardhan, S.V.; Sefcik, J. Scalable continuous solvothermal synthesis of metal organic framework (MOF-5) crystals. *Chem. Eng. J.* **2016**, *285*, 718. [CrossRef]
43. Cao, J.; Guo, C.; Chen, Z. Loading and release mechanisms of MOF-5@BTA-X (X=-CH_3/-NH_2/-$CO(CH_2)_6CH_3$): Experimental and theoretical investigations. *Colloids Surf. A Physicochem. Eng. Asp.* **2023**, *666*, 131274. [CrossRef]
44. Arjmandi, M.; Altaee, A.; Arjmandi, A.; Pourafshari Chenar, M.; Peyravi, M.; Jahanshahi, M. A facile and efficient approach to increase the magnetic property of MOF-5. *Solid. State Sci.* **2020**, *106*, 106292. [CrossRef]
45. Mohammadpour, Z.; Zare, H.R. The role of embedded 2-ABT@Cu-BTC MOF on the anti-corrosion performance of electro-assisted deposited silica sol-gel composite film. *Mater. Chem. Phys.* **2021**, *267*, 124590. [CrossRef]
46. Bennabi, S.; Belbachir, M. Synthesis and Characterization of New Organometallic Hybrid Material LCP-1 Based on MOF (Metal–Organic Framework) and Maghnite-H+, a Protons Exchanged Montmorillonite Clay, as Catalytic Support. *J. Inorg. Organomet. Polym. Mater.* **2017**, *27*, 1787–1799. [CrossRef]
47. Ramukutty, S.; Ramachandran, E. Crystal growth by solvent evaporation and characterization of metronidazole. *J. Cryst. Growth* **2012**, *351*, 47–50. [CrossRef]
48. Steckiewicz, K.P.; Cieciórski, P.; Barcińska, E.; Jaśkiewicz, M.; Narajczyk, M.; Bauer, M.; Kamysz, W.; Megiel, E.; Inkielewicz-Stepniak, I. Silver Nanoparticles as Chlorhexidine and Metronidazole Drug Delivery Platforms: Their Potential Use in Treating Periodontitis. *Int. J. Nanomed.* **2022**, *17*, 495. [CrossRef]
49. Minecka, A.; Tarnacka, M.; Jurkiewicz, K.; Hachuła, B.; Wrzalik, R.; Bródka, A.; Kamiński, K.; Kamińska, E. The impact of the size of acetylated cyclodextrin on the stability of amorphous metronidazole. *Int. J. Pharm.* **2022**, *624*, 122025. [CrossRef]
50. Tang, Z.G.; Callaghan, J.T.; Hunt, J.A. The physical properties and response of osteoblasts to solution cast films of PLGA doped polycaprolactone. *Biomaterials* **2005**, *26*, 6618–6624. [CrossRef]
51. Talelli, M.; Rijcken, C.J.F.; Lammers, T.; Seevinck, P.R.; Storm, G.; van Nostrum, C.F.; Hennink, W.E. Superparamagnetic Iron Oxide Nanoparticles Encapsulated in Biodegradable Thermosensitive Polymeric Micelles: Toward a Targeted Nanomedicine Suitable for Image-Guided Drug Delivery. *Langmuir* **2009**, *25*, 2060–2067. [CrossRef] [PubMed]

52. Sevim, K. *Modelling of Drug Release from Biodegradable Polymers*; University of Leicester: Leicester, UK, 2017.
53. Pitt, G.G.; Gratzl, M.M.; Kimmel, G.L.; Surles, J.; Sohindler, A. Aliphatic polyesters II. The degradation of poly (DL-lactide), poly (ε-caprolactone), and their copolymers in vivo. *Biomaterials* **1981**, *2*, 215–220. [CrossRef] [PubMed]
54. Tang, Z.G.; Rhodes, N.P.; Hunt, J.A. Control of the Domain Microstructures of PLGA and PCL Binary Systems: Importance of Morphology in Controlled Drug Release. *Chem. Eng. Res. Des.* **2007**, *85*, 1044–1050. [CrossRef]
55. Haynes, A.S.; Prinzi, A.; Silveira, L.J.; Parker, S.K.; Lampe, J.N.; Kavanaugh, J.S.; Horswill, A.R.; Fish, D. Cefadroxil Comparable to Cephalexin: Minimum Inhibitory Concentrations among Methicillin-Susceptible Staphylococcus aureus Isolates from Pediatric Musculoskeletal Infections. *Microbiol. Spectr.* **2022**, *10*, e01039-22. [CrossRef]
56. Dione, N.; Khelaifia, S.; Lagier, J.-C.; Raoult, D. The aerobic activity of metronidazole against anaerobic bacteria. *Int. J. Antimicrob. Agents* **2015**, *45*, 537–540. [CrossRef]
57. Brook, I.; Long, S.S. 187-Anaerobic Bacteria: Classification, Normal Flora, and Clinical Concepts. In *Principles and Practice of Pediatric Infectious Diseases*, 5th ed.; Long, S.S., Prober, C.G., Fischer, M., Eds.; Elsevier: Berlin/Heidelberg, Germany, 2018; pp. 987–995.e982.
58. Kumar, G.; Kant, A.; Kumar, M.; Masram, D.T. Synthesis, characterizations and kinetic study of metal organic framework nanocomposite excipient used as extended release delivery vehicle for an antibiotic drug. *Inorganica Chim. Acta* **2019**, *496*, 119036. [CrossRef]
59. Kumar, G.; Chaudhary, K.; Mogha, N.K.; Kant, A.; Masram, D.T. Extended Release of Metronidazole Drug Using Chitosan/Graphene Oxide Bionanocomposite Beads as the Drug Carrier. *ACS Omega* **2021**, *6*, 20433–20444. [CrossRef] [PubMed]
60. Lajevardi, A.; Sadr, M.H.; Yaraki, M.T.; Badiei, A.; Armaghan, M. A pH-responsive and magnetic Fe_3O_4@silica@MIL-100(Fe)/beta-CD nanocomposite as a drug nanocarrier: Loading and release study of cephalexin. *New J. Chem.* **2018**, *42*, 9690–9701. [CrossRef]
61. Murugapandian, R.; Clement, S.; Uthirapathy, V. Fabrication and In Vitro Drug Delivery Evaluation of Cephalexin Monohydrate-Loaded PLA:PVA/HAP:TiO_2 Fibrous Scaffolds for Bone Regeneration. *ACS Omega* **2023**, *8*, 5017–5032. [CrossRef]
62. Russell, D.L.; Uslan, D.Z.; Rubin, Z.A.; Grogan, T.R.; Martin, E.M. Multidrug Resistant Acinetobacter baumanii: A 15-Year Trend Analysis. *Infect. Control Hosp. Epidemiol.* **2018**, *39*, 608–611. [CrossRef]
63. Alzayn, M.; Dulyayangkul, P.; Satapoomin, N.; Heesom, K.J.; Avison, M.B. OmpF Downregulation Mediated by Sigma E or OmpR Activation Confers Cefalexin Resistance in Escherichia coli in the Absence of Acquired β-Lactamases. *Antimicrob. Agents Chemother.* **2021**, *65*, e01004-21. [CrossRef] [PubMed]
64. Japoni, A.; Ziyaeyan, M.; Jmalidoust, M.; Farshad, S.; Alborzi, A.; Rafaatpour, N.; Badiee, P. Antibacterial susceptibility patterns and cross-resistance of methicillin resistant and sensitive Staphyloccus aureus isolated from the hospitalized patients in Shiraz, Iran. *Braz. J. Microbiol.* **2010**, *41*, 567–573. [CrossRef] [PubMed]
65. Ramukutty, S.; Jeyasudha, R.; Ramachandran, E. Mechanical and thermal studies of metronidazole crystals. *Ind. J. Phys.* **2013**, *87*, 1001–1004. [CrossRef]
66. Pielichowski, K.; Majka, T.M. *Polymer Composites with Functionalized Nanoparticles: Synthesis, Properties, and Applications*; Elsevier: Amsterdam, The Netherlands, 2019.
67. Burke, T.L.; Rupp, M.E.; Fey, P.D. Staphylococcus epidermidis. *Trends Microbiol.* **2023**, *31*, 763–764. [CrossRef]
68. Ramia, N.F.; Tang, L.; Cocozaki, A.I.; Li, H. Staphylococcus epidermidis Csm1 is a 3′-5′ exonuclease. *Nucleic Acids Res.* **2014**, *42*, 1129–1138. [CrossRef]
69. Lewicki, M.; Kozioł, M.; Lorenc, K.; Kozioł, M.; Pawlicki, M.; Smoleń, A. Citrobacter freundii and Acinetobacter baumanii infection in a patient with neoplastic lung disease—Case report. *Ann. Agric. Environ. Med.* **2021**, *28*, 724–728. [CrossRef]
70. Laborel-Préneron, E.; Bianchi, P.; Boralevi, F.; Lehours, P.; Fraysse, F.; Morice-Picard, F.; Sugai, M.; Sato'o, Y.; Badiou, C.; Lina, G.; et al. Effects of the Staphylococcus aureus and Staphylococcus epidermidis Secretomes Isolated from the Skin Microbiota of Atopic Children on CD4+ T Cell Activation. *PLoS ONE* **2015**, *10*, e0141067. [CrossRef]

Disclaimer/Publisher's Note: The statements, opinions and data contained in all publications are solely those of the individual author(s) and contributor(s) and not of MDPI and/or the editor(s). MDPI and/or the editor(s) disclaim responsibility for any injury to people or property resulting from any ideas, methods, instructions or products referred to in the content.